Shivkant Thakur*, Rajan Mishra, Sanjay Kumar Soni and Praveen Kumar Rao

Crescent shaped slot loaded antenna sensor with tri-band notched for cancer detection

https://doi.org/10.1515/freq-2021-0240
Received October 14, 2021; accepted February 22, 2022;
published online March 15, 2022

Abstract: In this work, a unique tri-band notch and multi-band UWB antenna sensor has been designed for microwave sensing system to find out the cancerous tissues. The crescent shaped slot loaded antenna has been designed to avoid interferences between the antennas in UWB ranges. Using notches, the antenna sensitivity increases for detection. The proposed method has been verified through simulation and validated using measurements. S11 plot of the proposed antenna shows three notches at 3 GHz, 4.75 GHz and 7.25 GHz. It also shows four bands and omnidirectional radiation pattern over the UWB frequency range. Ground plane has been chosen to be hexagonal to achieve fourth band. I-shaped and U-shaped parasitics improve the antenna performance in third band. Crescent shaped and C-shaped slots improve the performance of first and second band of the antenna respectively. Additionally, phantom without tumors and with single and multiple tumors are fabricated. S-parameter analysis is a better approach to detect the cancerous tissues in the breast. Concept of principal component analysis of statistical machine learning has also been used to distinguish S-parameter of normal breast phantom from malignant breast phantom.

Keywords: breast cancer detection; crescent shaped slot loaded antenna (CSLA); microwave sensor; PCA; UWB antenna.

1 Introduction

Early identification of breast cancer has recently played an essential role in preventing early death among women around the world. In 2020, an estimated 2.26 million new cases have occurred which is about 0.17% more than the cases in 2018. According to WHO reports, 684,996 fatalities reported over the world. If they were diagnosed in the early stage, the risk reduction [1] would have been more, resulting in lesser fatalities. X-ray mammography, computed tomography (CT) scan, positron emission tomography (PET) scan, ultrasound and magnetic resonance imaging (MRI) techniques are the current screening modalities for early-stage cancer identification. The most commonly used and accepted methods for early recognition of breast cancer is x-ray mammography and PET scan. In spite of its success in detection, it has several shortcomings like lesser reliability, patient discomfort, ionized radiation, difficulties in detecting cancer in its early stage and a high false-alarm rate [2].

Existing imaging approaches such as MRI and CT can produce true images of high-resolution. These imaging methods are still large, massive, and slow. Therefore, such methods are not available in the countryside and in emergency vehicles like ambulances or at distant health clinics. All of these drawbacks point to the need for a supplemental breast imaging tool which is less bulky, less time-consuming and which may augment existing approaches. The use of microwave energy in imaging is currently attracting the attention of research community. Microwave detection systems are simple, safe, portable and cost effective [3]. At the microwave frequencies (300 MHz–300 GHz) of EM waves, the microwave imaging (MI) helps to distinguish and access the interior structure of any object. It is a development of previously used detection tactics which used MI technology in microwave tomography and radar-based imaging. It may be used for a variety of activities including structural health examination, medical imaging, non-destructive testing and evaluation etc. It has received recognition for its help to detect malicious cells in the breast also. In MI, the radiated signal from the antenna sensor is incident on the object under examination and scattered through it. Because malignant cells have a higher permittivity than normal cells, electromagnetic waves are scattered differently across them. The receiving antenna picks up the reflected back echo signal. The dielectric contrast between healthy and malignant tissues is used to identify tumours [4].

***Corresponding author: Shivkant Thakur**, Madan Mohan Malaviya University of Technology, Gorakhpur, India,
E-mail: shivkantjuet2k11@gmail.com
Rajan Mishra, Sanjay Kumar Soni and Praveen Kumar Rao, Madan Mohan Malaviya University of Technology, Gorakhpur, India,
E-mail: rajanmishra1231@gmail.com (R. Mishra),
sksoniec@mmmut.ac.in (S.K. Soni), rao.praveenmmmut@gmail.com (P.K. Rao). https://orcid.org/0000-0002-4170-5133 (R. Mishra)

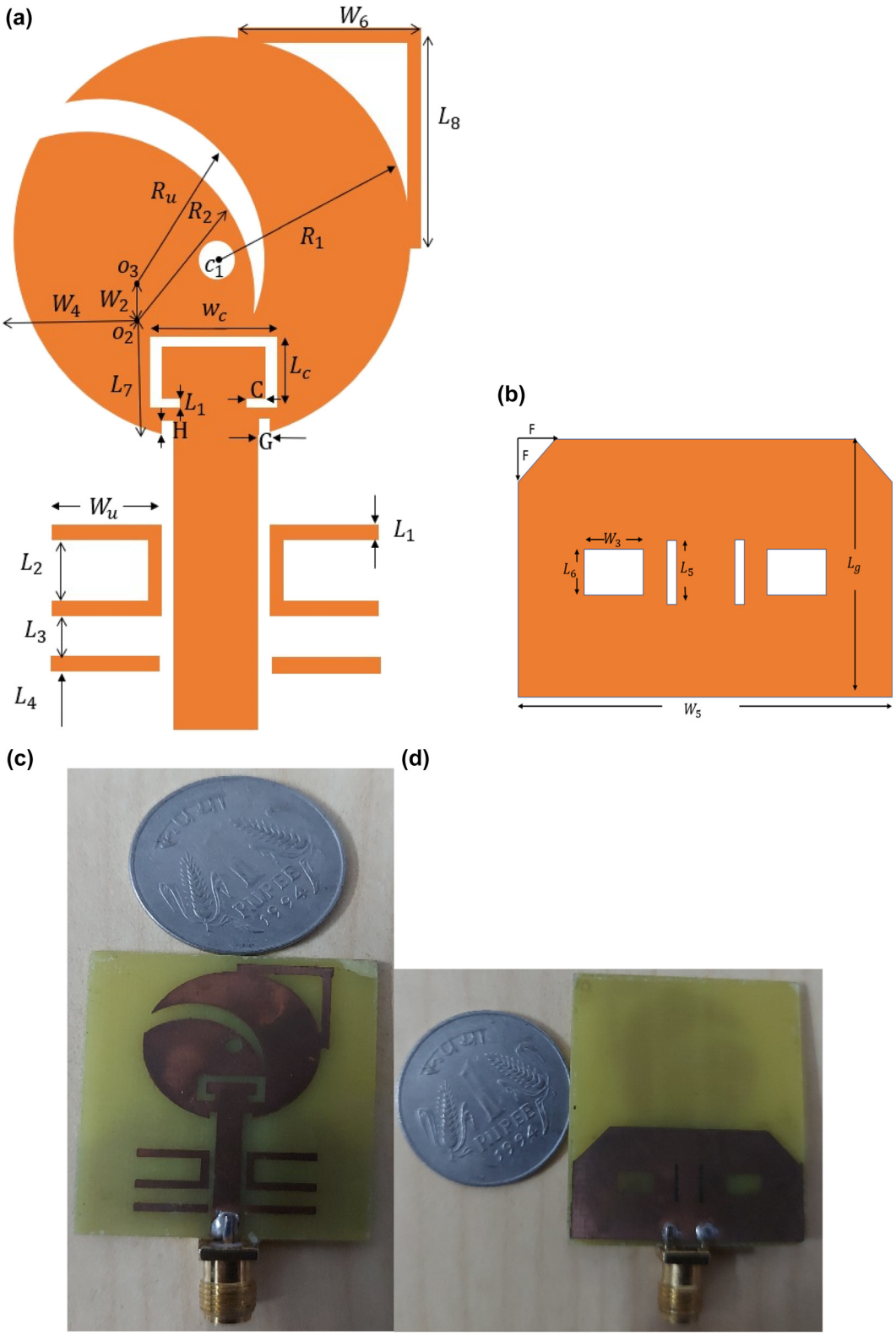

Figure 1. Simulated and fabricated antenna sensor. (a) Top view, (b) bottom view, (c) CSLA prototype of proposed antenna (top view), (d) CSLA prototype of proposed antenna (bottom view).

Different types of antennas are described in the literature which are used in imaging modalities for breast cancer diagnosis [4–11]. Sugitani et al. [4] proposed a 4 × 4 array antenna in the concern to operate in the range of 6–12.5 GHz but the antenna is not verified with spherical curvature shape of breast and does not cover all of the UWB bandwidth. Moreover, the antenna size is also quite larger. In elliptically slotted antenna, S-structured slot in feedline and C-structured parasitic stubs are used to generate the dual band notches. Using slots in feed line and asymmetrical parasitic, the achieved bandwidth has been of 8.37 GHz while the maximum gain of antenna is 4.08 dBi. However, the application of antenna has not been implemented in cancer detection [6]. In [7], elliptical shaped MIMO antenna has been designed with operating frequency band of 3.2–14 GHz. It has slotted ground plane and its radiation pattern has directional properties. However, the size of antenna is 16 × 71.5 × 0.254 mm^3 which is comparatively large. In [8], the antenna has an ultra-wideband of 120 percent and a frequency range from 3 GHz to 12 GHz with an overall size of 35 mm × 20 mm × 1.6 mm. But only four tumor locations were analyzed and also with a high SAR value. The detected tumor location was different from original position of the tumor. In square monopole patch antenna, a square radiating patch and a ground plane with a pair of horizontal T-shaped strips protruded inside the slot provides a wide fractional bandwidth of nearly 120% (2.97–12.83 GHz). The antenna achieves radiation efficiency of 86% and bandwidth of 9.86 GHz on dimension of 12 × 18 mm^2 [9]. The antenna shows omni-directional radiation pattern but gain of antenna is not given and not verified with the tumour. In [10], return loss characteristic of antenna covers the frequency range of 3–10 GHz. In entire frequency band, the antenna has stable and high-directional patterns as well as a narrow HPBW. In [11], UMAS sensor probe with 4 elements is operated within frequency range of 2.8–20 GHz for breast cancer detection.

In literatures, distinct approaches in microwave sensing are seen. In [12], three approaches are described for image formation that are active, passive, and hybrid. In [4], pulsed confocal and in [13] microwave-induced thermal acoustic tomography are discussed. In [14], confocal and in [15] a microwave imaging via space-time beamforming approach is presented. In [16], radar-based breast cancer is presented. When short UWB electromagnetic pulses are transmitted and received back at antenna, the scattering information is collected. In [17],

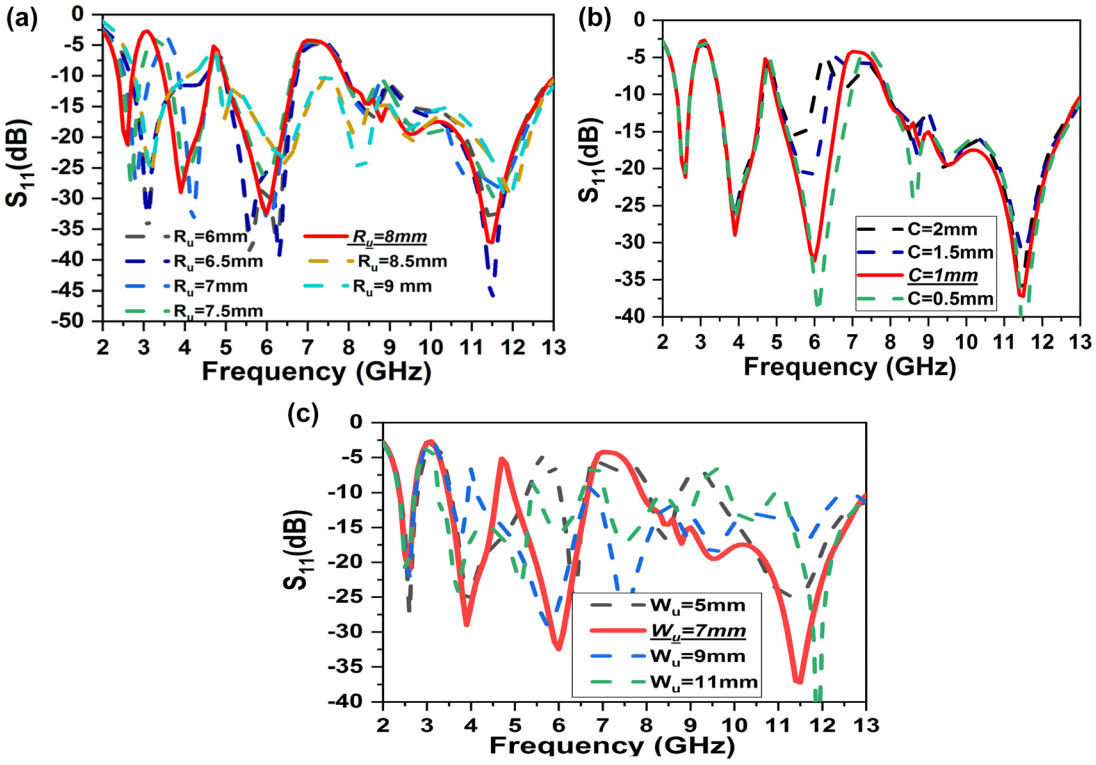

Figure 2. Parametric analysis of proposed design. (a) Parametric variation of crescent outer radius (R_u), (b) parametric variation of C-slot, (c) parametric variation of length of U-shaped parasitic.

nanoparticles based approach is discussed. In [18], near-field antenna and in [19], S-parameter data in the complex frequency domain are recorded. The core concept of this approach is that malicious breast tumours and normal breast tissues vary significantly in respect of their dielectric properties at microwave frequencies [20]. Non-ionizing radiation is used in this procedure, which is much better than the ionising radiation used in x-ray mammography in respect of human health. MI does not require compression thus making the examination more convenient than in case of mammography [14]. Regular screening is also made possible by this technology because of the low-illumination power levels used in the process. MI has the advantage of being quite inexpensive too.

In this paper, a novel UWB monopole crescent shaped slot loaded antenna (CSLA) sensor is proposed for the microwave sensor application. This antenna has four bands with three notches. Notches are provided to avoid interferences with existing narrow band communication application such as Wi-MAX (2.8–3.4 GHz), C-band (4.7–5 GHz) and downlink X-band (6.7–7.9 GHz). Moreover, the antenna thus becomes more sensitive for the tumor. Using antenna, S11 variation with a breast phantom can be recorded which indicates the location of

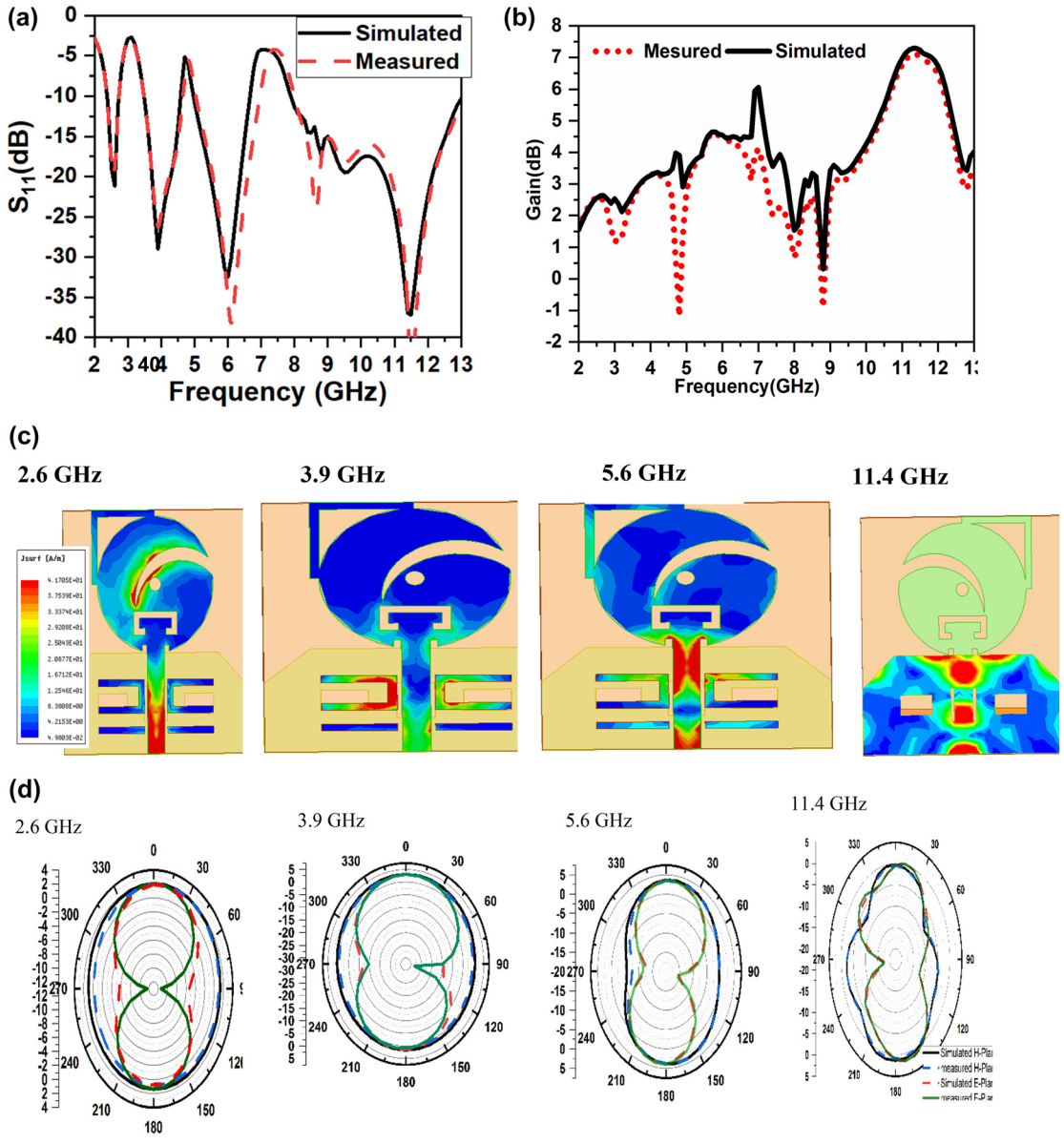

Figure 3: Simulation and measurement results, (a) S11 of proposed antenna (b) gain of proposed antenna, (b) current distribution at 2.6 GHz, 3.9 GHz and 6 GHz, 11 GHz, (c) radiation pattern at 2.6 GHz, 3.9 GHz, 6 GHz and 11.5 GHz in *E*–*H* plane.

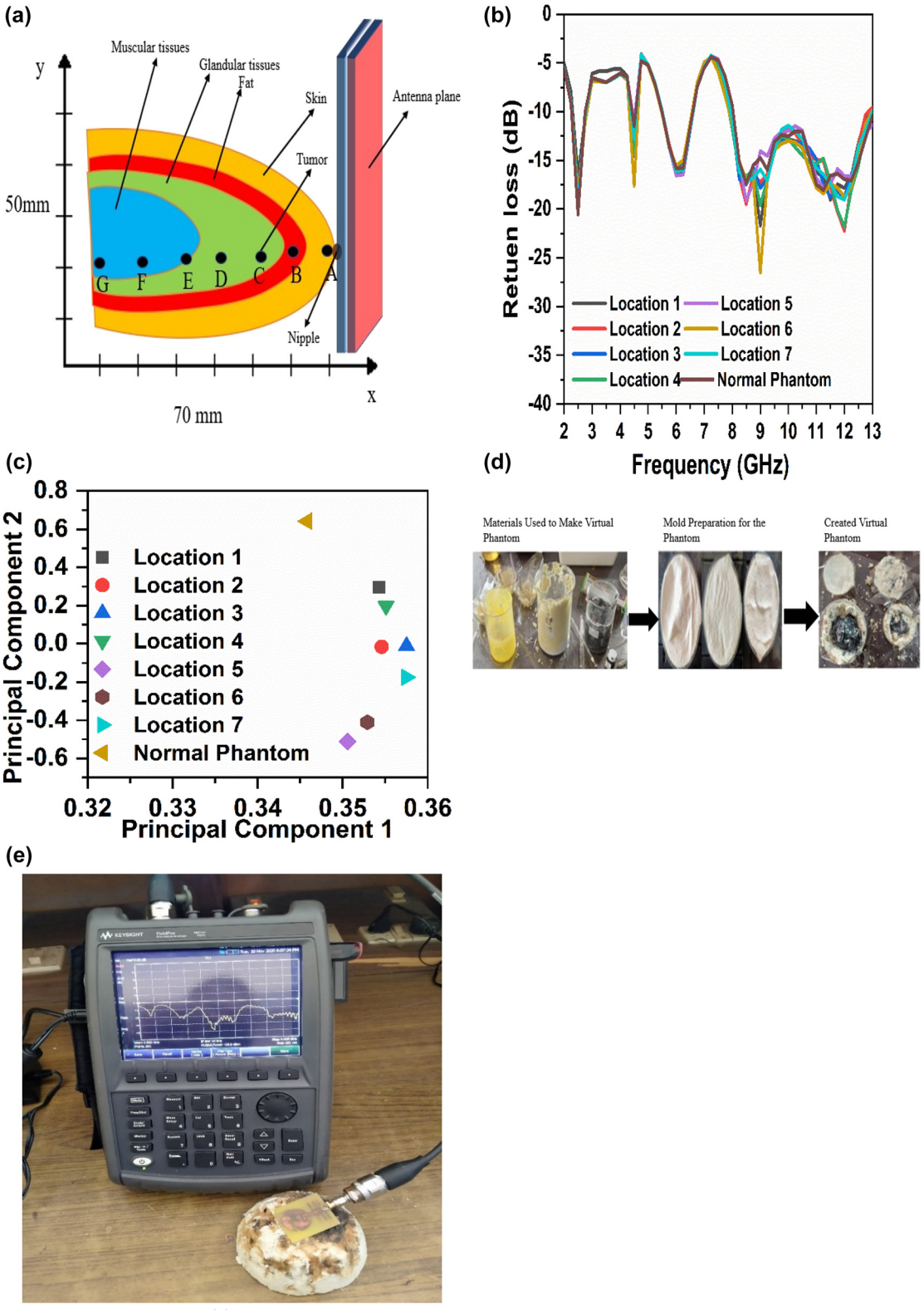

Figure 4: Breast phantom model preparation and result measurement. (a) Inner section of breast model with the positions of tumor, (b) simulated results of return loss at different positions of tumor, (c) variation in PCA value with tumor (d) phantom model development process, (e) measured result using developed phantom with antenna.

tumor. Defective ground structures improve the wideband characteristics mainly in the context of radar-based imaging techniques (e.g., [21–23]). Slot-loading techniques are used to reduce the size of antenna and produce four bands and triple notches within the UWB range [24]. This antenna sensor is using single port that reduces the system complexity. Also, the three notches in S-parameter results in more variation in reflected power that increases the sensitivity of the antenna sensor. These attentions lead to the prescribed characteristics in microwave sensing for the proposed antenna like compactness, simple to model and omnidirectional radiation pattern.

2 Antenna design

The geometry of proposed CSLA with triple notch bands is shown in Figure 1. The CSLA coated on the top of FR-4 substrate has loss tangent of 0.025, dielectric constant of 4.4 ($W_s \times L_s$), thickness of 1.6 mm and a microstrip feed line (3 mm × 15 mm). Defected ground structure (DGS) is engraved on the bottom side of the substrate to improve the bandwidth of CSLA. Introduction of slots in ground structure results in reduction of reflection from current surface. Thus, the impedance matching is maintained and return loss gets improved. DGS cut diagonally on the top vertex in triangular shape on each side results in negligible effect on S11 at low frequencies but it affects at higher frequencies. The DGS possesses symmetrical geometry across the microstrip feed line.

A circular patch introduced with defective ground results in an integrated UWB antenna. The crescent-shaped slot in the patch creates the first notch. U and I-shaped parasitics on the patch create the third band notch while the C-shaped slot in the patch affect the second notch.

The crescent slot and C slot are of length $\lambda/2$ of centre frequency and are given by this formula

$$f_{1,2\ \text{notch}} \approx \frac{c}{2L\sqrt{\epsilon_{\text{eff}}}} \tag{1}$$

Where f_{notch} notch frequency of the band, L is the total length of the slot and ϵ_{eff} is the effective dielectric constant which is given by $\epsilon_{\text{eff}} = \frac{\epsilon_r+1}{2}$ and L can be calculated as

For crescent shape slot, $L \approx \frac{2\pi R_2}{3} + \frac{2\pi R_u}{3}$ as the angle subtended at the center is 120°.

For C-Slot, $L = W_c + 2L_c + 2C$.

Two U-shaped parasitic strips are used to realise the rejected frequencies. The following formulas can be used to determine the dimensions.

$$L_{\text{parasitic}} \approx \frac{c}{f_{3\,\text{notch}}\sqrt{\epsilon_{\text{eff}}}} \tag{2}$$

Here, $L_{\text{parasitic}} = 2W_u + L_2$.

The performance of antenna depends on crescent outer radius that varies from 6 mm to 8 mm, as shown in Figure 2(a). At crescent outer radius 8 mm, the antenna performance has been optimized. First band is obtained at

Table 1: Dimensions of CSLA.

Variable	Dimensions (mm)	Variable	Dimensions (mm)
W_s, W_5	32	F, L_5, W_3	5
L_s	36	L_g	15
R_2, W_u	7	L_3, L_6, L_2, L_4	3
L_7	7.5	L_c	3.5
G	0.8	W_c	7.6
H	1.4	L_1, C	1
W_4	11.5	R_1	10.1
W_2	0.5	L_8, W_6	12
R_u	8		

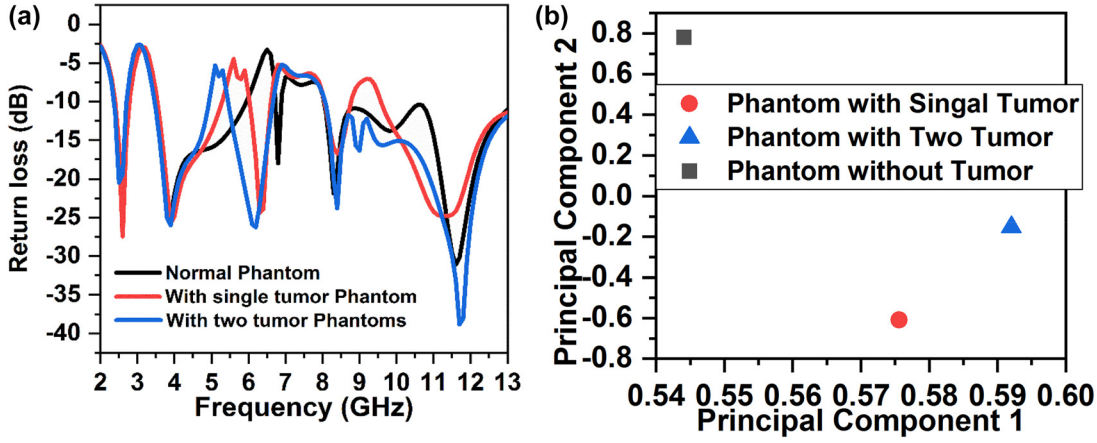

Figure 5. Measured reflection coefficients and PCA values with different phantoms. (a) Measured, reflection coefficients variation with frequency of different phantoms, (b) measured PCA values with phantoms.

the lower frequency of 2.6 GHz. Figure 2(b) shows the variation of C-slot from 0.5 mm to 2 mm and clearly shows the third band obtained at 1 mm of frequency 3.9 GHz. U-arm of parasitic varies from 5 mm to 11 mm as shown in Figure 2(c). The desired result is obtained at frequency of 6 GHz for the second band at 7 mm.

3 Results and discussions

Proposed antenna has four bands, first band of 2.35–2.78 GHz, second band of 3.46–4.65 GHz, third band of 5.08–6.08 GHz, and fourth band of 7.96–13 GHz. The resonance peaks at 2.6 GHz, 3.9 GHz, 5.6 GHz, and 11.4 GHz respectively are shown in Figure 3(a). In Figure 3(b), first peak is achieved at 2.7 GHz with gain of 2.13 dB, second peak at 4.1 GHz with gain 3.22 dB, third peak at 6.1 GHz with gain of 4.27 dB, and fourth peak at 11.2 GHz with gain of 7.13 dB. In Figure 3(c), the distribution of current depicts first resonance band due to the crescent shape slot cut out from patch. A parasitic of U-shaped, placed symmetrically around the microstrip feed line, creates second resonance band, third resonance band due to the C-slot cut out from the patch and fourth band due to hexagonal DGS. The simulated and measured radiation patterns are depicted in Figure 3(c). Proposed antenna provides a consistent and omnidirectional radiation pattern at lower frequency but as the frequency increases, the radiation pattern shifts from omnidirectional to directional. It shows an appreciable match between simulation and measurement results.

Table 2: Co-ordinates and their PC values.

Position Nos	Co-ordinates of tumor at (*x*, *y*) in mm	PC calues (PC1, PC2)
1	(10, 20)	(0.355, 0.3)
2	(20, 20)	(0.355, 0)
3	(30, 20)	(0.357, 0.08)
4	(40, 20)	(0.356, 0.2)
5	(50, 20)	(0.351, −0.5)
6	(60, 20)	(0.353, −0.4)
7	(70, 20)	(0.357, −0.1)

4 Phantom development of breast and detection process of tumor

Breast phantom model has been developed using four layers: skin, fat, glandular, and muscular. The simulation is carried out using HFSS software and the cancerous tumors are introduced at different location of the breast as depicted in Figure 4(a). The phantom model has been made heterogeneous using agar powder, distilled water, detergent, formalin, sodium chloride (NaCl), propylene glycol, polyethylene powder, xanthan gum [25]. Phantom models developed for the experiment are of three types: first is homogeneous normal phantom, second is homogeneous phantom with one tumor, while the third one is homogeneous phantom with two tumors. Prototype of phantom model with fabrication process setup for the detection of breast cancer [26] is depicted in Figure 4(d).

Vector network analyzer (VNA) of 85070E dielectric sample kit is being used for measurement of dielectric constant and tangent loss. In the experiment, electrical properties of breast phantom are obtained at seven different locations of different layers. The target value reaches as these seven data samples are averaged. The dielectric constant ranges for tumor tissue layers, skin, fat and gland tissue are 60–61, 34–40, 9–14, and 18–45 respectively and their conductivity ranges are 3.8–6.5, 1.5–2.5, 1.7–2.5, and 1.6–2.5 respectively [28].

4.1 PCA of reflection coefficient

Return loss of antenna has been measured by setting the antenna at the top of the simulated breast phantom. Further, the tumors have been placed between the

Table 3: Comparison table of proposed antenna sensor with existing research work.

References	Number of phantoms with which experiment performed	Maximum gain	Antenna types used in sensor	Size of antenna (mm^2)	Frequency range	Sensor results for analysis
[1]	Single	8.28 dB	Circular patch	28 × 37.5	2.59–10.32 GHz	Simulated SAR
[3]	Single	Not mentioned	Vivaldi antenna	110 × 95	1.6–3.02 GHz	S11 analysis
[5]	Two	Not mentioned	Slot antenna	44 × 52.4	3.5–15 GHz	GMP
[11]	Three	Not mentioned	4 elements UMAS	30 × 40	2.8–20 GHz	S11 analysis with PCA
[19]	Single	6.8 dBi	SSVA	45 × 37	3.9–9.15 GHz	PSF
Proposed	Three	7.13 dB	CSLA sensor	32 × 36	2.7–13 GHz	S11 analysis with PCA

Table 4: Comparison table of antenna with another notch antennas.

References	Bandwidth and antenna size	Notch bands	Peak Gain	Applications
[27]	3.1–14 GHz	4.2–6.2 GHz, 6.6–7.0 GHz and 12.2–14 GHz	Almost 8 dB	UWB cognitive radio communication
[28]	3.1–10.6 GHz	4.4–5 GHz, 5.1–5.9 GHz and 8.5–9 GHz	Almost 6 dBi	WLAN, satellite and military communication
[29]	2.8–11 GHz	5–6.3 GHz	Almost 5 dBi	–
[30]	2.7–12 GHz	3.4–3.69 GHz and 7.7–8.5 GHz	Almost 6 dBi	UWB applications
[31]	2.7–12 GHz	3.3–4.2 GHz	Almost 6 dBi	–
[32]	3–12.8 GHz	7.5–8.5 GHz	Almost 4 dBi	High-speed transmission of data
[33]	2.33–2.49 GHz, 5.7–5.9 GHz	–	2.2 dBi	WLAN applications.
Proposed	2.34–13 GHz	2.8–3.4 GHz, 4.7–5 GHz, and 6.7–7.9 GHz	7.13 dBi	Microwave antenna sensor

glandular layer and the fat at different positions from position 1 to position 7 as depicted in Figure 4(a). S11 data has been found in such a way, that it gives the locations of tumor at different positions. Further, variations in S11 parameters for various positions are depicted on a single point with the help of machine learning using PCA algorithm. The PCA has two components; principal component 1 and principal component 2. These seven positions with their PC values are tabulated as under in Table 1.

Normal phantom at position (0.345, 0.7) clearly differentiates between a malignant phantom and non-malignant phantom as shown in Figure 4(c).

Figure 5(a) shows the reflection coefficient of the antenna obtained by VNA for a normal phantom, single tumor phantom and double tumor phantom. This depicts quite small differences among the reflection curves of normal phantom, single and multiple tumors phantom. To recognize it correctly, PCA has been utilized on these reflection parameters. To differentiate between a normal and a benign tumor phantom, the principal component values of both the phantoms have been analyzed. PC values of normal phantom, single tumor and multi-tumor phantom are (0.54408, 0.77917), (0.57559, −0.60837) and (0.59204, −0.15092) respectively. Figure 5(b) shows that the tumor can be easily detected with the help of different PC values. Thus, the task to differentiate among the normal phantom, phantom with single and multiple tumors has been accomplished (Table 2).

In Table 3, a comparison between the proposed and researched work. Proposed CSLA sensor has verified with three different fabricated phantoms. The compact design, ultrawideband characteristics and S11 analysis using PCA makes sensor more sensitive for detecting tumors.

Comparison Table 4 shows the antennas with two ranges of bandwidth either 3–14 GHz or 2.7–12 GHz but the proposed antenna in this article has 2.34–13 GHz. In cancer detection, lower frequencies provide more depth of penetration and wider bandwidth facilitates for the higher resolution. Thus, the proposed antenna is better option for cancer detection.

5 Conclusions

A single compact radiating CSLA element has been proposed for detection of breast cancer. Crescent slot loaded antenna with simple and compact design operates in four bands and tri notch. Antenna sensor operates in the frequency range of 2.34–13 GHz with peak gain of 7.13 dB at frequency 11.2 GHz. Notch peaks are obtained at three frequencies: 3.1 GHz, 4.8 GHz, and 6.3 GHz. Three different heterogeneous breast phantom models have been developed for the experimental arrangement. After measurement, it is observed that electrical properties of both real breast and proposed phantom are nearly same. The difference between the power reflected from a malignant and a normal tissue with PCA technique becomes the foundation for the detection of cancer tissues. In this way, antenna becomes highly helpful in detection of deep laying cancerous tissues.

Author contributions: All the authors have accepted responsibility for the entire content of this submitted manuscript and approved submission.
Research funding: None declared.
Conflict of interest statement: The authors declare no conflicts of interest regarding this article.

References

[1] A. El Fatimi, S. Bri, and A. Saadi, "UWB antenna with circular patch for early breast cancer detection," *Telkomnika (Telecommunication Comput. Electron. Control.*, vol. 17, no. 5, pp. 2370–2377, 2019.

[2] W. A. Berg, L. Gutierrez, M. S. NessAiver, et al., "Diagnostic accuracy of mammography, clinical examination, US, and MR imaging in preoperative assessment of breast cancer," *Radiology*, vol. 233, no. 3, pp. 830–849, 2004.
[3] A. Filipe Lourenço Martins and I. Superior Técnico, *Antennas Design and Image Reconstruction for Microwave Imaging Systems*, Lisboa, Portugal, Instituto Superior T´ecnico, 2018, pp. 1–10.
[4] S. C. Hagness, A. Taflove, and J. E. Bridges, "Two-dimensional FDTD analysis of a pulsed microwave confocal system for breast cancer detection: fixed-focus and antenna-array sensors," *IEEE Trans. Biomed. Eng.*, vol. 45, no. 12, pp. 1470–1479, 1998.
[5] T. Sugitani, S. Kubota, A. Toya, X. Xiao, and T. Kikkawa, "A compact 4×4 planar UWB antenna array for 3-D breast cancer detection," *IEEE Antenn. Wireless Propag. Lett.*, vol. 12, pp. 733–736, 2013.
[6] V. N. K. R. Devana and A. M. Rao, "Design and analysis of dual band-notched UWB antenna using a slot in feed and asymmetrical parasitic stub," *IETE J. Res.*, pp. 1–11, 2020, https://doi.org/10.1080/03772063.2020.1816226.
[7] P. K. Rao and R. Mishra, "Elliptical shape flexible MIMO antenna with high isolation for breast cancer detection application," *IETE J. Res.*, pp. 1–9, 2020, https://doi.org/10.1080/03772063.2020.1819887.
[8] I. Amdaouch, O. Aghzout, A. Naghar, A. V. Alejos, and F. Falcone, "Breast tumor detection system based on a compact UWB antenna design," *Prog. Electromagn. Res. M*, vol. 64, pp. 123–133, 2018.
[9] N. Ojaroudi, M. Ojaroudi, and N. Ghadimi, "UWB omnidirectional square monopole antenna for use in circular cylindrical microwave," *IEEE Antenn. Wireless Propag. Lett.*, vol. 11, pp. 1350–1353, 2012.
[10] A. R. Celik and M. B. Kurt, "Development of an ultra-wideband, stable and high-directive monopole disc antenna for radar-based microwave imaging of breast cancer," *J. Microw. Power Electromagn. Energy*, vol. 52, no. 2, pp. 75–93, 2018.
[11] M. K. Sharma, M. Kumar, J. P. Saini, et al., "Experimental investigation of the breast phantom for tumor detection using ultra-wide band-MIMO antenna sensor (UMAS) probe," *IEEE Sensor. J.*, vol. 20, no. 12, pp. 6745–6752, 2020.
[12] K. L. Carr, "Microwave radiometry: its importance to the detection of cancer," *IEEE Trans. Microw. Theor. Tech.*, vol. 37, no. 12, pp. 1862–1869, 1989.
[13] L. V. Wang, X. Zhao, H. Sun, and G. Ku, "Microwave-induced acoustic imaging of biological tissues," *Rev. Sci. Instrum.*, vol. 70, no. 9, pp. 3744–3748, 1999.
[14] E. C. Fear, X. Li, S. C. Hagness, and M. A. Stuchly, "Confocal microwave imaging for breast cancer detection: localization of tumors in three dimensions," *IEEE Trans. Biomed. Eng.*, vol. 49, no. 8, pp. 812–822, 2002.
[15] E. J. Bond, S. Member, X. Li, S. Member, S. C. Hagness, and B. D. Van Veen, "Microwave imaging via space-time beamforming for early detection of breast cancer," *IEEE Trans. Antenn. Propag.*, vol. 51, no. 8, pp. 1690–1705, 2003.
[16] M. Klemm, I. J. Craddock, J. A. Leendertz, A. Preece, and R. Benjamin, "Radar-based breast cancer detection using a hemispherical antenna array – experimental results," *IEEE Trans. Antenn. Propag.*, vol. 57, no. 6, pp. 1692–1704, 2009.
[17] M. Farina, F. Piacenza, F. De Angelis, et al., "Broadband near-field scanning microwave microscopy investigation of fullerene exposure of breast cancer cells," *IEEE MTT-S Int. Microw. Symp. Dig.*, no. 12, pp. 4823–4831, 2016.
[18] J. M. Felicio, J. M. Bioucas-Dias, J. R. Costa, and C. A. Fernandes, "Antenna design and near-field characterization for medical microwave imaging applications," *IEEE Trans. Antenn. Propag.*, vol. 67, no. 7, pp. 4811–4824, 2019.
[19] M. Z. Mahmud, M. T. Islam, M. Samsuzzaman, S. Kibria, and N. Misran, "Design and parametric investigation of directional antenna for microwave imaging application," *IET Microw, Antennas Propag.*, vol. 11, no. 6, pp. 770–778, 2017.
[20] M. M. Islam, M. T. Islam, M. R. I. Faruque, M. Samsuzzaman, N. Misran, and H. Arshad, "Microwave imaging sensor using compact metamaterial UWB antenna with a high correlation factor," *Materials*, vol. 8, no. 8, pp. 4631–4651, 2015.
[21] X. Li, S. C. Hagness, M. K. Choi, and D. W. Van Der Weide, "Numerical and experimental investigation of an ultrawideband ridged pyramidal horn antenna with curved launching plane for pulse radiation," *IEEE Antenn. Wireless Propag. Lett.*, vol. 2, pp. 259–262, 2003.
[22] W. Huang and A. A. Kishk, "Compact dielectric resonator antenna for microwave breast cancer detection," *IET Microw, Antennas Propag.*, vol. 3, no. 4, pp. 638–644, 2009.
[23] J. Bourqui, M. Okoniewski, and E. C. Fear, "Balanced antipodal Vivaldi antenna with dielectric director for near-field microwave imaging," *IEEE Trans. Antenn. Propag.*, vol. 58, no. 7, pp. 2318–2326, 2010.
[24] M. A. Al-joumayly, S. M. Aguilar, S. C. Hagness, and N. Behdad, "Multi-band, miniaturized patch antenna elements for microwave breast imaging applications," *IEEE Antenn. Wireless Propag. Lett.*, vol. 9, pp. 268–271, 2010.
[25] P. K. Rao and R. Mishra, "Resonator based antenna sensor for breast cancer detection," *Prog. Electromagn. Res. M*, vol. 101, pp. 149–159, 2021.
[26] M. T. Islam, M. Samsuzzaman, S. Kibria, and M. T. Islam, "Experimental breast phantoms for estimation of breast tumor using microwave imaging systems," *IEEE Access*, vol. 6, pp. 78587–78597, 2018.
[27] Y. Li, W. Li, and Q. Ye, "A reconfigurable triple-notch-band antenna integrated with defected microstrip structure band-stop filter for ultra-wideband cognitive radio applications," *Int. J. Antenn. Propag.*, vol. 2013, pp. 1–13, 2013.
[28] Y. Li, W. Li, and W. Yu, "A switchable UWB slot antenna using SIS-HSIR and SIS-SIR for multi-mode wireless communications applications," *Appl. Comput. Electromagn. Soc. J.*, vol. 27, no. 4, pp. 340–351, 2012.
[29] C. Liu, T. J. Yingsong Li, and X. Yang, "Miniaturization cantor set fractal ultrawideband antenna with a notch band characteristic," *Microw. Opt. Technol. Lett.*, vol. 54, no. 5, pp. 1227–1230, 2012.
[30] Y. Li and W. Li, "A compact CPW-FED circular slot antenna with reconfigurable dual band-notch characteristics for UWB communication applications," *Microw. Opt. Technol. Lett.*, vol. 55, no. 11, pp. 2562–2568, 2014.

[31] Y. Li and W. Li, "A compact circular slot UWB antenna with multimode reconfigurable band-notched characteristics using resonator and switch techniques," *Microw. Opt. Technol. Lett.*, vol. 56, no. 3, pp. 570–574, 2014.
[32] Y. Li and W. Li, "Miniaturization of asymmetric coplanar STRIP-FED staircase ultrawideband antenna with reconfigurable notch band," *Microw. Opt. Technol. Lett.*, vol. 55, no. 7, pp. 1467–1470, 2013.
[33] Y. Li and W. Li, "A compact asymmetric coplanar strip-fed dual-band antenna for 2.4/5.8 GHz WLAN applications," *Microw. Opt. Technol. Lett.*, vol. 55, no. 9, pp. 2066–2070, 2013.